PHYSICAL REVIEW E **99**, 010103(R) (2019)

Rapid Communications

Liquid state anomalies and the relationship to the crystalline phase diagram

Domagoj Fijan and Mark Wilson
Department of Chemistry, Physical and Theoretical Chemistry Laboratory, University of Oxford, South Parks Road, Oxford OX1 3QZ, United Kingdom

(Received 11 September 2018; published 10 January 2019)

A relationship between the observation of a density anomaly and the underlying crystalline phase diagram is demonstrated. The crystal phase diagram and temperature of maximum density (TMD) lines are calculated over a range of parameter space using a Stillinger-Weber potential. Relationships between the *loci* of density maxima in the PT plane for the liquid state and the underlying crystalline phase diagram are investigated. Two key potential parameters are systematically varied in order to control the balance between the model two- and three-body interaction terms, and the relative effects of varying the potential parameters analyzed. The respective TMD lines diverge at extreme values with one set of lines showing a reentrant behavior. For each parameter set the TMD lines are extrapolated to $T = 0$ K. The corresponding pressures are related to the crystalline phase diagram and are found to lie on or near specific crystal-crystal coexistence lines for a wide range of potential parameters. The density anomaly is observed to vanish corresponding to regions in the crystal phase diagram which lack crystal-crystal coexistence lines potentially offering a new interpretation for the emergence of anomalous behavior.

DOI: 10.1103/PhysRevE.99.010103

The origin of anomalous behavior in liquids is a long-standing mystery in the field of condensed matter and, significantly, in the water community. Although exhaustive thermodynamical studies have been performed [1] and significant progress made, no unified theory as to the origin of anomalous behavior exists. Recently the focus has shifted toward studying the relationship between anomalies and liquid structure [2–6]. The two-state model has, for example, proved to be successful in tackling many of the intricacies of this problem [7] leading to the identification of specific local environments that relate to the observed anomalous behavior. To date there has been relatively little work which considers any relationship between the coexistence lines on the crystalline phase diagram and lines that define the thermodynamic anomalies [8,9]. Previous work relies on the observation that the systems which show anomalies have more than one clearly related and thermodynamically accessible crystal structure [8,9].

Crystalline (highly ordered) and amorphous or liquid (disordered) structures may be reasonably expected to show significant similarities. However, connections between the evolution of liquid structure with state point (which is generally continuous) and any underlying crystalline phase transformations (which are generally discontinuous) are often unclear. Clear links should be possible given that the interactions in the different states are likely to be similar (in the absence of, e.g., traversing a metal-insulator transition). Extensions of the phase diagram into the thermodynamically metastable regimes (e.g., on supercooling) may uncover a richness of phase behavior, showing distinct amorphous regions which differ in density and show well-defined phase boundaries [10]. A prevalent characteristic is a balance between forming relatively low-density ("open") structures at low pressures and significantly higher density ("close-packed") structures at higher pressures. This balance is mirrored in the crystalline phase diagram and in the metastable supercooled amorphous regimes. Furthermore, systems of this type often display pressure-induced amorphization in which an amorphous structure is generated directly from a crystal on application of pressure [11–13]. Network systems (e.g., Si, Ge, H_2O, SiO_2, GeO_2, and BeF_2) also often display anomalous properties which may extend into both the structure and dynamics. Of these, perhaps the most well-known anomaly is in the density of H_2O (see, e.g., Ref. [13], and references therein). Constructing a locus of the turning points (usually in the PT or ρT planes) generates a temperature of maximum density (TMD) line. Further anomalies are observed in, for example, the heat capacity, isothermal compressibilities, and diffusivities [13–30]. The origins and relationships between these anomalies appear complex, potentially arising from a subtle disruption of the tetrahedral network and have been studied using accurate models for SiO_2 [18,19,26,29], BeF_2 [27–29], GeO_2 [29], and H_2O [3,6,13,15–17,29,31] and their evolution traced using the Stillinger-Weber potential [32,33] and using ramp [26,34–36] or core-softened [37] potentials. Potential models, in which the energy of interaction is deconvoluted into a series of n-body ($n \geqslant 2$) interactions are attractive both for their relative simplicity (computational efficiency) and for the ability to control fundamental interactions in a well-defined manner. For example, many of the issues outlined above may be considered insightfully using potential models in which the two- and three-body interactions are determined explicitly and their relative magnitudes varied.

In this work we present systematic numerical evidence for the conditions under which the density anomaly emerges in systems modeled with a Stillinger-Weber (SW) potential [38]. The purpose of this work is to outline that the origin of anomalous behavior can be traced back to elementary properties of the underlying crystalline phase diagram rather than relying on a more standard "hunt" for the source of this behavior (e.g., searching for the liquid-liquid critical point). We systematically explore the liquid and crystalline phase space and the model parameter space by tuning two different physically intuitive parameters in the SW model. The SW model is a widely used potential that can effectively model a range of monatomic systems which are based on local tetrahedral geometries, including silicon [38], phosphorus [39,40], germanium [41], carbon [42], water [43], and even a range of multicomponent systems [40,44,45]. Here we extend the studies to nontetrahedral local environments, offering the possibility of exploring a range of additional systems. We focus on the TMD lines as a signature of significant structural change in the disordered environment and consider their relationship to the underlying crystalline phase diagram by extrapolating to $T = 0$ K in order to uncover links with the crystalline phase diagrams as well as relating to changes in the local structure. A Stillinger-Weber potential [38] is employed throughout as an example of a well-studied model *known* to show key anomalous properties and in which the relative strengths of the two- and three-body terms is easily controlled [32,33,41,46–49]. The two key parameters varied (labeled λ and θ_0) control the strength of the three-body term and the preferred local bond angle. The effect of varying λ (with θ_0 set at the ideal tetrahedral angle, θ_{T_d}) has been considered previously [32,33,41,46–48] whilst the effect of varying θ_0 has been less well studied [49]. A study using a somewhat different model (a Kern-Frenkel model [50]) which focused on the liquid-liquid critical point progression as a function of the angle of interaction has been reported [51].

Figure 1 shows the crystal phase diagrams obtained at $T = 0$ K both as a function of λ and θ_0 with all other parameters fixed at the values used to model silicon [38]. The phase diagrams are constructed by determining the energy and volume curves for each potential crystal structure. For structures which show either orthorhombic or tetragonal symmetry, different ratios of unit cell lengths are considered and the lowest free energy at a given volume identified. The system pressure is calculated from the derivative of the energy which allows the free energy to be evaluated and coexistence lines to be constructed. A useful feature of this approach is that the results are exact in the limit that all the possible crystal structures can be assessed. Consider first the ideal tetrahedral potential model ($\theta_0 = \theta_{T_d}$) as a function of λ [Fig. 1(a)]. At high λ the diamond crystal structure becomes stable, reflecting the relatively large energetic penalty imposed on local configurations which deviate from the ideal tetrahedron. For $\lambda < 27$ a richer phase diagram emerges in which the thermodynamically stable crystal structures reflect a balance between the close-packed and more open structures favored by the two- and three-body interactions, respectively. At (small) negative pressures the low-density clathrate (SII and SIII) structures are stable. At positive pressures the BC8, SC16, and o-X crystal structures become stable. These all have distorted tetrahedral nearest-neighbor topologies with a relatively short next-nearest- (fifth) neighbor length scale [52–56]. The o-X crystal structure has been recently characterized [56] (having been first observed theoretically [54]) and can be considered as a distorted β-Sn crystal structure. The SC16 and BC8 crystal structures are closely related and hence occupy similar regions of the phase diagrams. The figures also highlight the regions for which the SC16 structure is thermodynamically stable over the diamond structure but metastable with respect to BC8. At low λ structures with nearest-neighbor coordination numbers greater than four become stable (bcc at low pressure, simple cubic at high pressure) reflecting the increased dominance of the two-body interactions. Figure 1(b) shows the phase diagram at fixed λ ($\lambda = 21$) as a function of the local geometry parameter, θ_0. Figures 1(a) and 1(b)

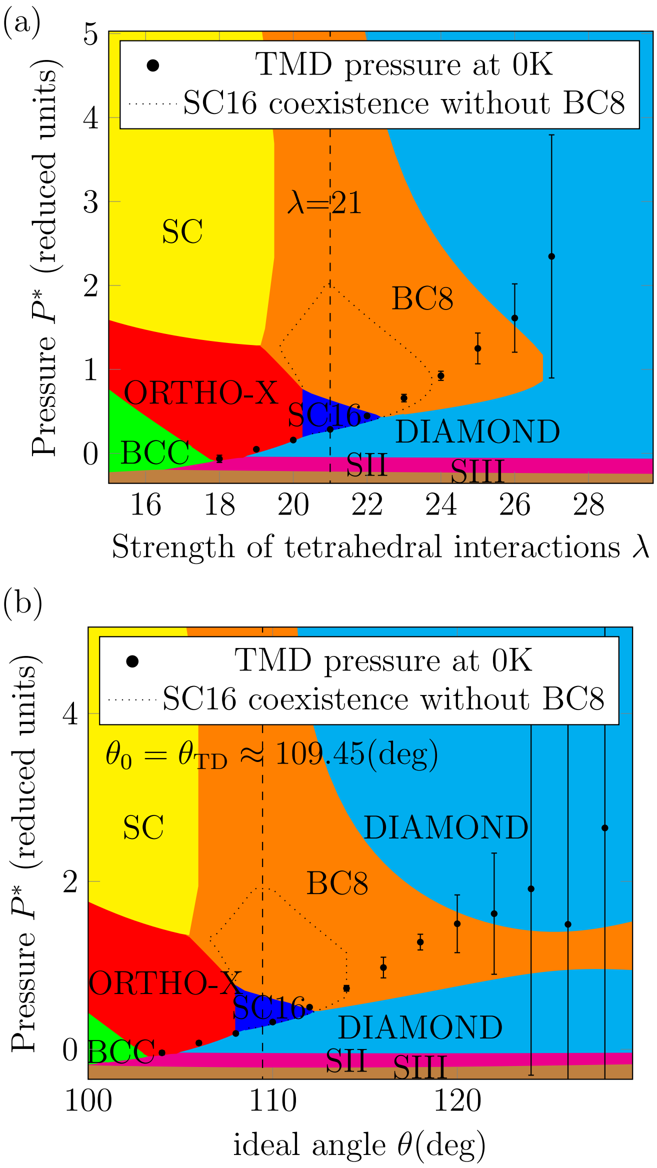

FIG. 1. Crystal phase diagrams determined at $T = 0$ K for the Stillinger-Weber potential and shown as a function of the reduced pressure, p^*, as a function of (a) the magnitude of the three-body interaction energy (as controlled by the parameter λ), and (b) the favored angle formed by atoms in the local coordination polyhedra (as controlled by the parameter θ_0). The dotted lines highlight the regions in which the SC16 crystal structure is thermodynamically stable over the diamond structure but metastable with respect to the BC8 structure. The dashed lines highlight the $\theta_0 = \theta_{T_d}$ and $\lambda = 21$ lines, respectively, and which represent the line of intersection of the two phase diagrams. In both cases the solid circles highlight the extrapolation of the TMD lines (shown in Fig. 2) to $T = 0$ K as described in the text.

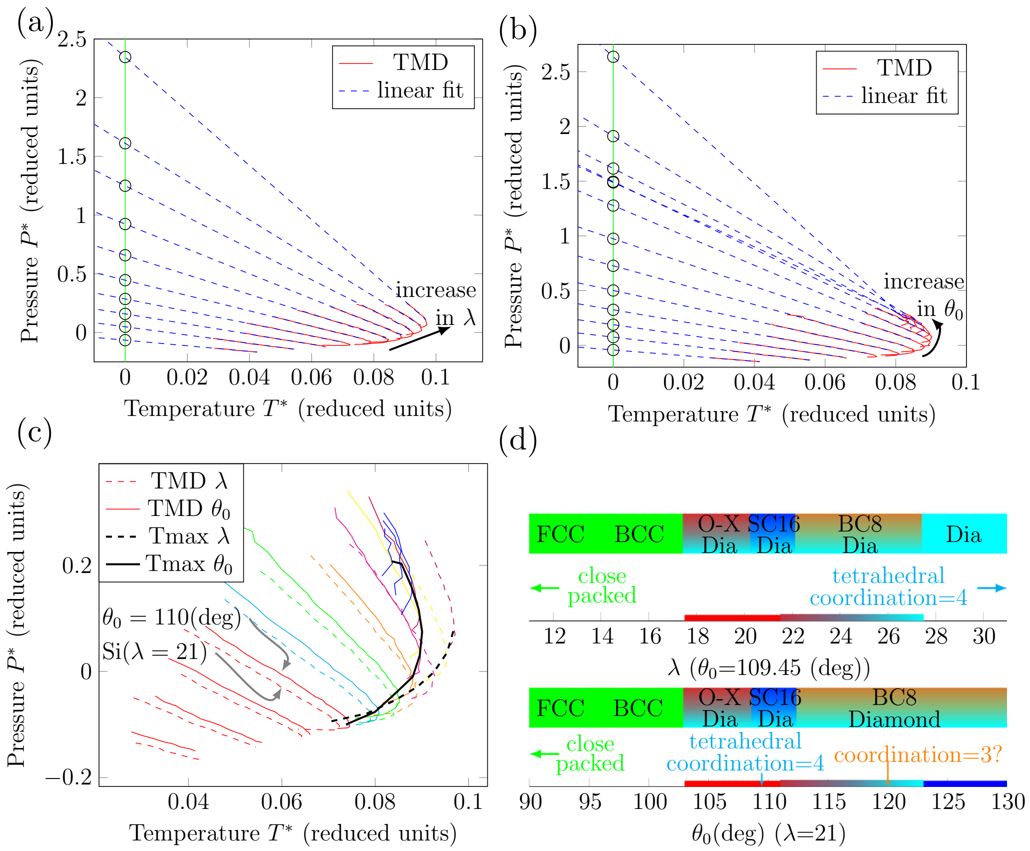

FIG. 2. Temperature of maximum density (TMD) lines determined using a Stillinger-Weber potential and varying (a) λ (fixing $\theta_0 = \theta_{T_d}$) and (b) θ_0 (fixed $\lambda = 21$) shown as a function of reduced pressure, P^*, and temperature, T^*. In panel (a) successive TMD lines are shown for $\lambda = 18$–27 (in unit increments) as highlighted, whilst in panel (b) successive lines are shown for $\theta_0 = 104$–128° (in increments of 2°). In both panels (a) and (b) the dashed lines show fits to the linear sections of the TMD lines which are used to extrapolate to $T = 0$ K. (c) Comparison of the progression of the TMD lines for different values of λ (dashed) and θ_0 (solid). The TMD lines at relatively low temperature show the same trend as a function of either λ or θ_0, in which increasing the respective parameters shifts the TMD lines to higher pressures and temperatures. At higher temperature the differently shaded TMD lines highlight the onset of divergent behavior with increasing λ or θ_0. The solid (dark) blue TMD lines at high pressures show a progression with increasing θ_0 for which no λ counterpart has been identified. For these the temperature dependence of the TMD lines appears inverted in that increasing θ_0 shifts the lines to lower temperatures and higher pressures. The thick solid black lines show the respective envelopes of the maximum temperatures of each TMD line and so highlight the differing evolution of these lines with increasing λ and θ_0. (d) Summary of the key density anomaly behavior observed for varying λ (upper panel) and θ_0 (lower panel). The lower text indicates the local structures observed in the amorphous phase and the upper text the stable crystal phase at $T = 0$ K and at the TMD pressure. The lines on the axis follow the shading scheme from (c) denoting different behavior of the TMD progression. For the crystal phases the single shaded regions identify single crystal phases whilst the graduated shades denote regions where coexistence between two crystal phases is important. The shading follows the scheme of Fig. 1.

intersect at $\lambda = 21$, $\theta_0 = \theta_{T_d}$ (as highlighted by dashed vertical lines) and appear to map onto each other at low $\Delta\theta$ ($=\theta_0 - \theta_{T_d}$) of $\sim 10^\circ$. At first impression this mapping may appear obvious as, in a Stillinger-Weber potential, the total energy is expressed as a sum of explicit two- and three-body terms and the magnitude of the latter is controlled both by λ and θ_0. However, the dependence of the energy on the deviation from θ_0 is approximately quadratic (compared to the linear dependence on λ). However, although the dependence of the three-body energy term is even about θ_0, reducing θ_0 will tend to favor the two-body energy term (as the system can adopt a relatively high coordination number). As a result, lowering θ_0 is equivalent in some sense to lowering λ. At high $\Delta\theta$ ($>10^\circ$) clear differences in the phase diagrams emerge, for example in the greater range of the stability field for the BC8 structure.

Figure 2 shows the loci of the temperatures at which the system density reaches a maximum, shown in the PT plane for (a) varying λ ($\theta_0 = \theta_{T_d}$) and (b) varying θ_0 ($\lambda = 21$). A point is generated by performing simulations at fixed volumes, varying the temperature, and locating the pressure and temperature at which $(\partial P/\partial T)_V = 0$. At fixed θ_0 [Fig. 2(a)] TMD lines are observed for $18 \leqslant \lambda \leqslant 27$ and shift to higher pressure and temperature as the strength of the three-body interaction increases (reflecting the behavior of the underlying liquid-gas spinodals [47]). For fixed λ [Fig. 2(b)] a slightly different behavior emerges with TMD lines observed for $104^\circ \leqslant \theta_0 \leqslant 128^\circ$. For $104^\circ \leqslant \theta_0 \leqslant 120^\circ$ the TMD lines show analogous behavior to those for increasing λ, with successive curves shifting to higher temperature and pressure. For $\theta_0 \geqslant 120^\circ$ the TMD curves retrace to lower temperature whilst increasing in pressure. To highlight the differences associated with changing both λ and θ_0, Fig. 2(c) shows the respective TMD lines combined. The low λ and θ_0 curves effectively map onto each other. However, as both parameters increase the TMD lines diverge with those associated with changes in θ_0 showing a reentrant behavior, shifting to lower temperature as the pressure increases. The TMD progression is consistent in both λ and θ_0 at low λ (<22) and θ_0 (<112°). The onset of divergent behavior begins at intermediate λ ($21 < \lambda < 28$) and θ_0 ($110^\circ < \theta_0 < 124^\circ$) and is highlighted in the colored graduation in Figs. 2(c) and 2(d). At high λ the density anomaly vanishes but is retained for high θ_0. Reducing λ favors more close-packed structures, which will also be the case for reducing θ_0 below θ_{T_d}. Increasing λ further stabilizes the four-coordinate (tetrahedral) sites. However, increasing θ_0 "pushes" the favored structures away from both the close-packed and tetrahedral environments. These observations are summarized in Fig. 2(d).

The TMDs shown in Fig. 2 are extrapolated to $T = 0$ K by identifying the near-linear regimes and fitting a line using a least-squares procedure. Ideally, we would study the TMD-crystal coexistence relations at finite temperatures. However, assessing a vast range of possible crystal phases at finite temperatures for a wide range of λ and θ_0 is potentially highly complex. For example, avoiding thermally driven phase transitions between competing crystal structures (and so obtaining metastable extensions to crystal-liquid coexistence curves) may be problematic. The solution proposed here is to consider the TMD extrapolation to $T = 0$ K at which we can determine the phase diagram exactly for a wide range of possible crystal structures. The extrapolation of the TMD to low temperature is not without concerns, however. The limit of the high-pressure TMD locus can terminate in three ways. In the first the line may collide with the $T = 0$ K line (the singularity-free scenario [16]). The gradient of the TMD locus in the PT projection should start to increase as the temperature is lowered. In the second case the TMD may merge with the temperature of *minimum* density anomaly locus [57]. By construction this must occur at zero gradient in the PT projection which means that the TMD has to increase in gradient. In the third scenario the TMD locus may collide with the spinodal line emanating from the liquid-liquid critical point [15] or the second liquid-gas critical point [13]. In this scenario an increase in gradient for the TMD locus is also observed. All three possibilities predict an increase in gradient for the TMD locus. However, as we do not know the exact functional form of the TMD line we opt to perform a linear extrapolation in order to obtain an upper pressure limit. Figure 1 shows these extrapolations projected onto the phase diagrams in terms of λ [Fig. 1(a)] or θ_0 [Fig. 1(b)]. TMD lines are not observed for $\lambda < 18$ and $\theta_0 < 104^\circ$, respectively, corresponding to the onset of the bcc crystal stability fields. Furthermore, TMD lines are not observed for $\lambda > 27$, in excess of the BC8 crystal stability field [Fig. 1(a)]. TMD lines *are* observed for high θ_0 in line with the increased BC8 crystal stability field [Fig. 1(b)]. In both cases the extrapolated pressures lie close to the respective diamond–o-X and diamond-SC16 coexistence curves for low and intermediate $\{\lambda, \theta_0\}$, respectively. For $\lambda \gtrapprox 22$ and $\theta_0 \gtrapprox 112^\circ$ the extrapolated TMD points approximately follow the SC16-diamond coexistence curves extended into the regions for which SC16 is metastable with respect to the BC8. For $\lambda \gtrapprox 24$ or $\theta_0 \gtrapprox 114^\circ$ these points no longer follow a clear coexistence curve but traverse the BC8 stability field. TMD lines are only observed across parameter space for which a nondiamond crystal structure shows a stability field. At high λ ($\lambda \gtrapprox 27$) the diamond crystal structure becomes favored across the whole (positive) pressure range studied. At high θ_0 the relative destabilization of *both* the close-packed and tetrahedral local coordination environments results in a

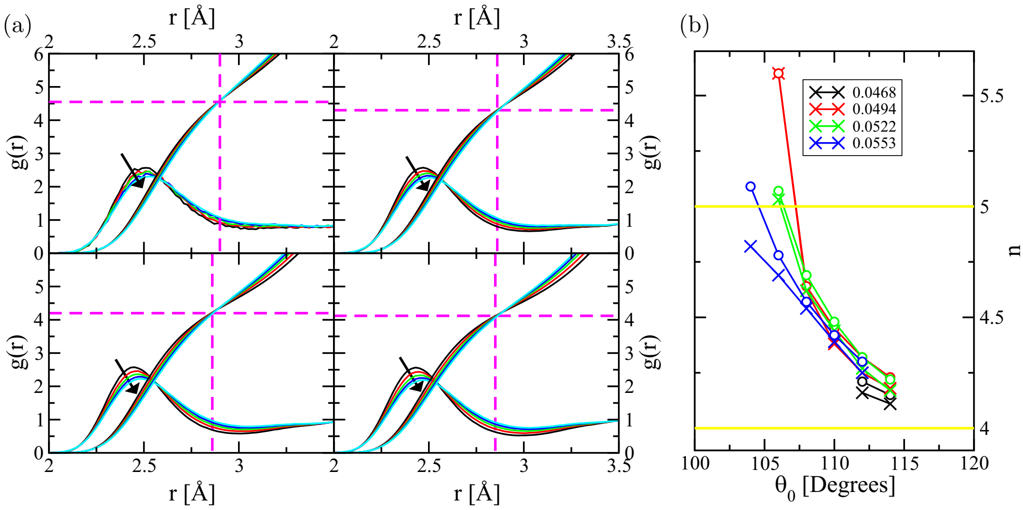

FIG. 3. (a) Radial distribution functions calculated at temperatures around the TMD at fixed density ($\rho = 0.0494$ Å^{-3}) for $\theta_0 = 108^\circ$ (top left), 110° (top right), 112° (bottom left), and 114° (bottom right), respectively. Functions are shown at temperatures around the TMD temperature of $\Delta T = -200$, -100, 0, 100, and 200 K (equivalent to -0.008, -0.004, 0, 0.004, and 0.008 in reduced units, respectively) (moving along the directions of the arrow as indicated). The figures also show the running coordination numbers, $n = 4\pi\rho\int_0^r r^2 g(r)dr$. Each set shows an isosbestic point, highlighted with the dashed lines in each panel. (b) Coordination number at the TMD with cutoff corresponding to the isosbestic point, shown as a function of both ρ and θ_0. The light horizontal lines highlight the coordination number range of 4–5.

BC8 crystal structure thermodynamic stability field which traverses the whole parameter range studied and, as a result, TMD lines are observed across this range.

A common probe employed to evaluate evolution in structure is the radial distribution function (RDF). Figure 3 shows the RDFs and running coordination numbers $[n(r_c) = 4\pi\rho \int_0^{r_c} r^2 g(r)dr]$ for four values of θ_0 (at fixed $\lambda = 21$). For each value of θ_0 five functions are shown which cover a range of $\Delta T = \pm 200$ K (equivalent to ± 0.008 in reduced units) around the temperatures of maximum densities. At each value of θ_0 the functions show an isosbestic point (a separation at which the coordination number curves approximately intersect) [4,58]. The presence of these points indicates that, at fixed density, there appears an "optimum" number of atoms within a given cutoff which is approximately temperature independent. Models which show extensive TMD lines have isosbestic coordination numbers in the range $4 < n_{\mathrm{iso}} < 5$ supporting the view that the key to these anomalies is the relationship between the fourth and fifth nearest neighbors [5]. The divergent behavior of the TMD lines at high λ and θ_0 can now be further rationalized. The high temperatures and pressures associated with the TMD lines for these high parameter values support more close-packed structures. However, higher θ_0 stabilizes lower coordination environments than high λ and so the overall coordination number remains closer to four at high θ_0 compared with high λ. The coordination number remains in the critical 4–5 range over a wider θ_0 parameter range than for λ.

To develop a more finely tuned view of the changes in local coordination environment we evaluate the difference in the mean separations of the fourth and fifth nearest neighbors, $\Delta r_{45} = r_5 - r_4$, *normalized* by r_5. Figures 4(a) and 4(b) show the evolution of Δr_{45} as a function of pressure for the TMD lines calculated at different values of λ and θ_0, respectively. The values of Δr_{45} increase as both λ and θ_0 increase. The figures also show the corresponding ambient pressure Δr_{45} values for the key crystal structures (which show stability fields in Fig. 1). The o-X, BC8, and SC16 crystals show values of Δr_{45} consistent with those observed for the TMD lines. The clear implication of Figs. 3 and 4, therefore, is that the existence of the TMD relies upon a fine balance between open (networklike) structures (here dominated by four-coordinate sites) and close-packed structures (here identified by the move toward the inclusion of the fifth nearest neighbor into the first coordination shell).

In this work we have demonstrated a correlation between the existence and location of the TMD anomalies in a relatively simple potential model which presents a potentially novel way of rationalizing the origin of the anomalous behavior in liquids. There is a relationship between the TMD lines and the crystal-crystal coexistence curves with the relative distances between the fourth and fifth nearest-neighbor atoms emerging as the key metric. In addition we have reported the limiting values of the potential parameters λ and θ_0 for which the density anomaly emerges.

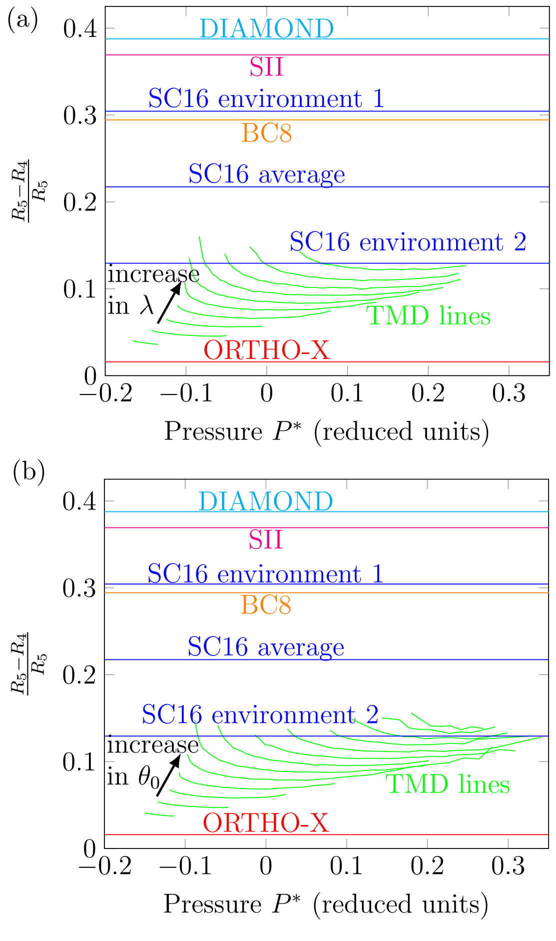

FIG. 4. The distance between the fourth and fifth nearest-neighbor atoms, $\Delta r_{45}[=(r_5 - r_4)/r_5]$, determined at the respective TMDs as a function of reduced pressure, p^*, and "normalized" by the fifth nearest-neighbor separation, r_5. The upper and lower panels show Δr_{45} as a function of θ and λ_0, respectively. The respective ($T = 0$ K) values for the SC16, BC8, SII, diamond, and o-X crystals, determined at $p^* = 0$, are shown for comparison. The SC16 crystal shows two such distances and their respective values and the weighted average are shown here.

This paper conforms to the RCUK data management requirements.

D.F. is grateful to St. Edmund Hall and the Clarendon Fund (University of Oxford) for financial support. We are grateful for support from the EPSRC Centre for Doctoral training, Theory and Modeling in Chemical Sciences, under Grant No. EP/L015722/1.

---

[1] P. Gallo, K. Amann-Winkel, C. A. Angell, M. A. Anisimov, F. Caupin, C. Chakravarty, E. Lascaris, T. Loerting, A. Z. Panagiotopoulos, J. Russo, J. A. Sellberg, H. E. Stanley, H. Tanaka, C. Vega, L. Xu, and L. G. M. Pettersson, Chem. Rev. **116**, 7463 (2016).

[2] R. Shi, J. Russo, and H. Tanaka, Proc. Natl. Acad. Sci. USA **115**, 9444 (2018).

[3] A. Nilsson and L. G. M. Pettersson, Nat. Commun. **6**, 8998 (2015).

[4] L. B. Skinner, C. J. Benmore, J. C. Neuefeind, and J. B. Parise, J. Chem. Phys. **141**, 214507 (2014).

[5] J. Russo and H. Tanaka, Nat. Commun. **5**, 3556 (2014).

[6] D. Nayar and C. Chakravarty, Phys. Chem. Chem. Phys. **15**, 14162 (2013).

[7] J. Russo, K. Akahane, and H. Tanaka, Proc. Natl. Acad. Sci. USA **115**, E3333 (2018).

[8] H. Tanaka, Phys. Rev. B **66**, 064202 (2002).

[9] G. Franzese, G. Malescio, A. Skibinsky, S. V. Buldyrev, and H. E. Stanley, Phys. Rev. E **66**, 051206 (2002).

[10] P. F. McMillan, G. N. Greaves, M. Wilson, M. C. Wilding, and D. Daisenberger, Polyamorphism and liquid-liquid phase transitions in amorphous silicon and supercooled Al_2O_3-Y_2O_3 liquids, in *Liquid Polymorphism* (Wiley, New York, 2013), pp. 309–353.

[11] D. Machon, F. Meersman, M. Wilding, M. Wilson, and P. McMillan, Prog. Mater. Sci. **61**, 216 (2014).

[12] S. Sastry and C. Austen Angell, Nat. Mater. **2**, 739 (2003).

[13] P. G. Debenedetti, J. Phys.: Condens. Matter **15**, R1669 (2003).

[14] S. Sastry, F. Sciortino, and H. E. Stanley, J. Chem. Phys. **98**, 9863 (1993).

[15] P. H. Poole, F. Sciortino, U. Essmann, and H. E. Stanley, Nature (London) **360**, 324 (1992).

[16] S. Sastry, P. G. Debenedetti, F. Sciortino, and H. E. Stanley, Phys. Rev. E **53**, 6144 (1996).

[17] J. R. Errington and P. G. Debenedetti, Nature (London) **409**, 318 (2001).

[18] M. S. Shell, P. G. Debenedetti, and A. Z. Panagiotopoulos, Phys. Rev. E **66**, 011202 (2002).

[19] I. Saika-Voivod, F. Sciortino, and P. H. Poole, Phys. Rev. E **63**, 011202 (2000).

[20] A. Mudi and C. Chakravarty, J. Phys. Chem. B **108**, 19607 (2004).

[21] A. Mudi and C. Chakravarty, J. Phys. Chem. B **110**, 4502 (2006).

[22] A. Mudi, C. Chakravarty, and R. Ramaswamy, J. Chem. Phys. **122**, 104507 (2005).

[23] A. Mudi, C. Chakravarty, and R. Ramaswamy, J. Chem. Phys. **124**, 069902 (2006).

[24] A. Mudi, C. Chakravarty, and E. Milotti, J. Chem. Phys. **125**, 074508 (2006).

[25] R. Sharma, A. Mudi, and C. Chakravarty, J. Chem. Phys. **125**, 044705 (2006).

[26] R. Sharma, S. N. Chakraborty, and C. Chakravarty, J. Chem. Phys. **125**, 204501 (2006).

[27] M. Agarwal, R. Sharma, and C. Chakravarty, J. Chem. Phys. **127**, 164502 (2007).

[28] M. Agarwal and C. Chakravarty, J. Phys. Chem. B **111**, 13294 (2007).

[29] B. S. Jabes, M. Agarwal, and C. Chakravarty, J. Chem. Phys. **132**, 234507 (2010).

[30] B. Shadrack Jabes, D. Nayar, D. Dhabal, V. Molinero, and C. Chakravarty, J. Phys.: Condens. Matter **24**, 284116 (2012).

[31] G. A. Cisneros, K. T. Wikfeldt, L. Ojamäe, J. Lu, Y. Xu, H. Torabifard, A. P. Bartók, G. Csányi, V. Molinero, and F. Paesani, Chem. Rev. **116**, 7501 (2016).

[32] V. Molinero, S. Sastry, and C. A. Angell, Phys. Rev. Lett. **97**, 075701 (2006).

[33] W. Hujo, B. S. Jabes, V. K. Rana, C. Chakravarty, and V. Molinero, J. Stat. Phys. **145**, 293 (2011).

[34] M. R. Sadr-Lahijany, A. Scala, S. V. Buldyrev, and H. E. Stanley, Phys. Rev. Lett. **81**, 4895 (1998).

[35] N. B. Wilding and J. E. Magee, Phys. Rev. E **66**, 031509 (2002).

[36] H. M. Gibson and N. B. Wilding, Phys. Rev. E **73**, 061507 (2006).

[37] E. Salcedo, A. B. de Oliveira, N. M. Barraz, C. Chakravarty, and M. C. Barbosa, J. Chem. Phys. **135**, 044517 (2011).

[38] F. H. Stillinger and T. A. Weber, Phys. Rev. B **31**, 5262 (1985).

[39] J.-W. Jiang, T. Rabczuk, and H. S. Park, Nanoscale **7**, 6059 (2015).

[40] J.-W. Jiang, Nanotechnology **26**, 315706 (2015).

[41] M. H. Bhat, V. Molinero, E. Soignard, V. C. Solomon, S. Sastry, J. L. Yarger, and C. A. Angell, Nature (London) **448**, 787 (2007).

[42] A. S. Barnard and S. P. Russo, Mol. Phys. **100**, 1517 (2002).

[43] V. Molinero and E. B. Moore, J. Phys. Chem. B **113**, 4008 (2009).

[44] A. Béré and A. Serra, Philos. Mag. **86**, 2159 (2006).

[45] Z. Q. Wang, D. Stroud, and A. J. Markworth, Phys. Rev. B **40**, 3129 (1989).

[46] M. Singh, D. Dhabal, A. H. Nguyen, V. Molinero, and C. Chakravarty, Phys. Rev. Lett. **112**, 147801 (2014).

[47] D. Dhabal, C. Chakravarty, V. Molinero, and H. K. Kashyap, J. Chem. Phys. **145**, 214502 (2016).

[48] C. A. Angell and V. Kapko, J. Stat. Mech. (2016) 094004.

[49] S. Saw, N. L. Ellegaard, W. Kob, and S. Sastry, Phys. Rev. Lett. **103**, 248305 (2009).

[50] N. Kern and D. Frenkel, J. Chem. Phys. **118**, 9882 (2003).

[51] F. Smallenburg, L. Filion, and F. Sciortino, Nat. Phys. **10**, 653 (2014).

[52] J. Crain, S. J. Clark, G. J. Ackland, M. C. Payne, V. Milman, P. D. Hatton, and B. J. Reid, Phys. Rev. B **49**, 5329 (1994).

[53] J. Crain, R. O. Piltz, G. J. Ackland, S. J. Clark, M. C. Payne, V. Milman, J. S. Lin, P. D. Hatton, and Y. H. Nam, Phys. Rev. B **50**, 8389 (1994).

[54] K. Akahane, J. Russo, and H. Tanaka, Nat. Commun. **7**, 12599 (2016).

[55] F. Romano, J. Russo, and H. Tanaka, Phys. Rev. B **90**, 014204 (2014).

[56] D. Fijan and M. Wilson, Chem. Phys. Lett. **685**, 316 (2017).

[57] P. G. Debenedetti and M. C. D'Antonio, AIChE J. **34**, 447 (1988).

[58] L. Bosio, S. H. Chen, and J. Teixeira, Phys. Rev. A **27**, 1468 (1983).